RESPONSE OF DARK-ADAPTED RETINAL ROD PHOTORECEPTORS

H. KHANAL[1], V. ALEXIADES[2], AND E. DIBENEDETTO[3]

[1] Department of Mathematics, Embry-Riddle Aeronautical University, Daytona Beach, FL 32114.
[2] Department of Mathematics, University of Tennessee, Knoxville, TN 37996-1300 and Oak Ridge National Laboratory, Oak Ridge TN 37831.
[3] Department of Mathematics, Vanderbilt University, Nashville TN 37240.

ABSTRACT.
The process of phototransduction, whereby light is converted into an electrical response, in rod and cone photoreceptors in the retina, involves as a key step, the diffusion of the cytoplasmic signaling molecules cGMP (cyclic guanosime monophosphate) and Ca^{2+} (Calcium ions), termed second messengers. The rod outer segment of vertebrates is a right circular cylinder housing about 1000 parallel, coaxial, equispaced, thin cylinders termed lipidic discs. The second messengers cGMP and Ca^{2+} diffuse in the cytoplasm (the fluid surrounding the discs). The complex geometry of the rod creates computational difficulties. We present spatio–temporal computational models for interactions and diffusion of cGMP and Ca^{2+} in the cytoplasm of vertebrate rod photoreceptors, as well as numerical simulations of the response to light of dark–adapted Salamander rods.
AMS (MOS) Subject Classification. 92C45, 35K60, 65Y05.

1. INTRODUCTION

1.1. Basic Mechanism of Phototransduction. The rod outer segment of vertebrates comprises a stack of equispaced *disc* membranes of thickness about 14 nm and at mutual distance of about 14 nm (for Salamander). Each disc is made up of two functionally independent layers of lipidic membrane where proteins are embedded, such as rhodopsin (Rh), the light receptor, G protein (G), also called transducin, and cGMP phosphodiesterase (PDE), the effector. These membrane associated proteins can diffuse on the face of the disc where they are located, but cannot abandon the disc. The lateral membrane of the rod contains cGMP–gated channels of small radius. In absence of light, these channels are open and allow a positive influx of sodium and calcium (Ca^{2+}) ions. The space within the rod, and not occupied by the discs, is filled with fluid cytosol, in which cyclic-guanosine monophosphate (cGMP) and Ca^{2+} diffuse.

When a photon is absorbed by a molecule of rhodopsin, located on one of the discs, the rhodopsin becomes activated and in turn activates any G protein it interacts with. Each of the activated G proteins is capable of activating one and only one catalytic subunit of PDE on the activated disc, by binding to it upon contact. The bound pair so generated is denoted by PDE*. This cascade takes place only on the activated disc. The next cascade, involving cGMP and Ca^{2+}, takes place in the cytosol. Active PDE* hydrolyzes cGMP in the cytoplasm, thereby lowering its concentration. The decrease of cGMP concentration causes closure of some of the cGMP–gated channels of the plasma membrane, resulting in a lowering of the influx of positive ions, and thus a lowering of the local current J across the outer membrane. Because the $Na^+/K^+/Ca^{2+}$ exchanger continues to remove Ca^{2+} from the cytoplasm, there is a decrease in the calcium concentration, which in turn results in an increase in cGMP production by stimulation of Ca^{2+}–inhibited guanylyl cyclase, and thus a consequent reopening of the channels. The same decrease of calcium closes the cycle by causing deactivation of rhodopsin through stimulation of rhodopsin kinase, which ceases activating new G protein. Thus PDE* decays to basal, ending depletion of cGMP (Pugh & Lamb, 2000).

1.2. **Basic Issues.** A *dark adaptated* rod is at a state of equilibrium in darkness. All fluxes of cGMP and Ca^{2+} are zero, their concentration is constant and there is a steady *dark current* J_{dark} across the plasma membrane of the rod outer segment. Physiologists are interested in the cellular *response* (defined as $J_{dark} - J$, with J the total circulating current) after the rod is exposed to light. The main computational difficulty of the problem is the intricate geometry of the cytosol. The issue of determining a consistent set of parameters for predictive modeling is also paramount.

1.3. **Overview.** Phototransduction has been studied extensively in recent years. The basic mechanism is now understood at a molecular level, but its formal mathematical description is less developed. Classically the basic signaling processes are investigated in terms of bulk averaged quantities (Pugh & Lamb, 2000), and ordinary differential equations provide solutions which average concentrations within the volume of the cell. However, it is becoming increasingly clear from recent investigations that several signaling molecules reside at specific sites within cells or their membranes and depend on their localization effects in a significant manner (Leskov et al., 2000). Therefore to analyse the regulation process quantitatively, one should take into account the local concentrations and time-dependent diffusion of second messengers and protein cascades.

We present theoretical and computational spatio–temporal models of the diffusive transport of cGMP and Ca2+ in the cytosol, their interaction with the disc bound effector PDE*, and the electrical current in response to photons. The models incorporate the main mechanisms presently known to operate in phototransduction, and reduce to simpler models proposed by physiologists. Namely they reduce to the longitudinal (one-dimensional) model of Gray-Keller et al. (1990) by assuming radially uniform concentrations, and to the lumped model (Nikonov et al., 1998; Nikonov et al., 2000; Pugh & Lamb, 2000) under the assumption of uniform (bulk) concentrations. The numerical simulations trace the space–time evolution of cGMP and Ca^{2+}, in terms of which the current through the plasma membrane can be computed. Thus, the simulation also provides the distribution of current as a space–time function defined on the lateral boundary of the rod outer segment. It exhibits localization of the response about the activation site and enables us to quantify the longitudinal spread at any particular time.

2. MATHEMATICAL MODELS

2.1. **Geometry.** The outer segment of a photoreceptor rod in vertebrates can be considered as a right circular cylinder $\tilde{\Omega}$ of height H and radius $R + \sigma\varepsilon_o$ (where R, σ, ε_o and H are positive numbers), housing a vertical stack of N equispaced parallel discs C_j, $j = 1, 2, \cdots N$, each of radius R, thickness ε_o, and mutually separated by a distance $\nu\varepsilon_o$ (Fig.1). Each of the discs C_j, carrying the rhodopsin, is assumed to be a thin cylinder of radius R and height ε_o, coaxial with the rod $\tilde{\Omega}$. The domain of cytosol Ω where diffusion of second messengers takes place is a region in the rod not occupied by the discs, i.e., $\Omega = \tilde{\Omega} - \bigcup_{j=1}^{N} \bar{C}_j$. We denote by $F_j^{\pm}$ the upper/lower disc faces, and by $\partial_o\Omega$ the lateral outer boundary (plasma membrane). The indicated geometry implies that, $N\varepsilon_o = H/(1 + \nu)$. We define $\theta_o := \text{vol}\left(\bigcup_{j=1}^{N} C_j\right)/\text{vol}(\Omega) = 1/(1 + \nu)$.
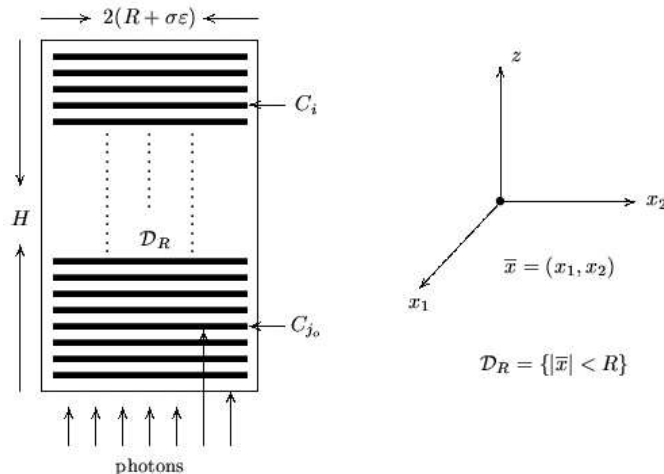

FIGURE 1. Schematic drawing of the rod outer segment

2.2. **Basic Equations of the Model.** Let u and w denote dimensionless concentrations of the second messengers cGMP and Ca^{2+} respectively. We rescale lengths and time so that various parameters, H, R, ε_o, . . . , and independent variables r, z, t, are all dimensionless. Employing cylindrical coordinates, the mathematical model for the diffusion of second messengers u and w in cytosol is expressed, in dimensionless form, as follows (Andreucci et al. 2003a; Khanal, 2003). Given $u(r, z, \theta, 0) = u_o$, $w(r, z, \theta, 0) = w_o$ with $u_o > 0$, $w_o > 0$, the initial uniform steady-state for the dark adapted system, find $u(r, z, \theta, t)$, $w(r, z, \theta, t)$ for $0 < t < \tau$, such that

$$(1) \qquad \frac{\partial u}{\partial t} - \nabla \cdot (D_u \, \nabla u) \; = \; 0, \qquad \frac{\partial w}{\partial t} - \nabla \cdot (D_w \, \nabla w) \; = \; 0,$$

in Ω, for $t > 0$, where D_u and D_w are the respective (dimensionless) diffusion coefficients.

Consider a beam of photons hitting a disc C_{j_o} on one of its faces, say for example the lower one, $F_{j_o}^-$, at coordinate z_o along the axis of the rod. Generation and removal of free cGMP in the cytoplasm occurs through binding phenomena on the lower and upper faces $F_j^\pm$ of each disc C_j. Calcium enters or leaves the cytosol only through $\partial_o \Omega$, the plasma membrane (via the cGMP-gated channels and the electrogenic exchanger). Thus the two parabolic partial differential equations in (1) are coupled weakly via the following nonlinear boundary conditions:

$$(2a) \qquad -D_u \frac{\partial u}{\partial z} \;=\; \pm \frac{1}{2} \nu \varepsilon_o \left\{ (C_{\min} + C_1 \, f_1(w)) - C_2 \, u \right\} + \delta_{jo} \, C_0 \, P \, u \quad \text{on} \quad F_j^\pm, \ t > 0,$$

$$(2b) \qquad -D_w \frac{\partial w}{\partial r} \;=\; g_1(w) \, - \, C_{\text{ratio}} \, g_2(u) \quad \text{on} \ \partial_o \Omega, \ t > 0,$$

where C_{ratio}, $C_{\min}$, C_1, C_2 and C_0 are positive constants expressing various interaction rates (such as rates of synthesis or hydrolysis of cGMP, etc, see Andreucci et al. 2003a; Khanal et al. 2003). The quantity P represents the strength of PDE*- cGMP interaction, and thus the effect of activation by light. $\delta_{j_0} = 1$ only when C_{j_0} is an activated disc, and zero otherwise. The fluxes on the remaining parts of the boundary of Ω are zero. The functions f_1, g_1 and g_2 are given by

$$(3) \qquad f_1(w) = \frac{1}{1 + (\gamma w)^{m_{\text{Ca}}}}, \qquad g_1(w) = \frac{w}{1 + w}, \qquad g_2(u) = \frac{u^{m_{\text{cG}}}}{1 + u^{m_{\text{cG}}}},$$

where γ is a constant related to the channel opening and the cyclace rate, and m_{Ca}, m_{cG} are Hill constants ($6.5 \leq \gamma \leq 16$, $m_{\text{Ca}} \approx 2$, $m_{\text{cG}} = 2$).

The quantities of primary interest to physiologists are the cG-gated, J_{cG}, and exchanger, J_{ex}, circulating currents, described by the following Hill and Michaelis-Menten type relations (Nikonov et al. 2000; Pugh & Lamb, 2000)

$$(4) \qquad J_{\text{cG}} = j_{\text{cG}}^{\max} g_2(u) \qquad \text{and} \qquad J_{\text{ex}} = j_{\text{ex}}^{\text{sat}} g_1(w),$$

where $j_{\text{cG}}^{\max}$ is the maximal cG-gated current, $j_{\text{ex}}^{\text{sat}}$ is the saturation exchanger current. The local current J at a point of the plasma membrane (with local concentrations u, w at that point) is the sum $J_{\text{cG}} + J_{\text{ex}}$.

2.3. **Activation Mechanism.** Light activation is embodied in the term $\delta_{jo} \, C_0 \, P \, u$ in (2b). A satisfactory full modeling of the function $P(x, t)$, for x ranging over a face $F_{j_0}^-$ hit by a photon, is a major open problem and one of the future goals of our investigation. The literature contains various attempts to describe such a quantity (see Koutalos et al. 1995; Pugh & Lamb, 2000; Nikonov et al. 2000; Hamer, 2000; Andreucci et al. 2003a; Khanal et al. 2003).

Here we consider a simple activation mechanism with a lumped model, by taking the surface density of activated PDE molecules as the total PDE* in the rod divided by the area of activated disc(s), namely,

$$(5) \qquad P(t) = \text{PDE}^*(t) / \left(N_{\text{active}} \cdot \pi R^2 \right),$$

where $\text{PDE}^*(t)$ is the number of activated PDE molecules in the entire rod and N_{active} is the number of activated discs. Following Nikonov et al. (1998), Pugh & Lamb (2000), the quantity $\text{PDE}^*(t)$ in (5) is approximated in terms of two first-order rate constants k_{R}, k_{E}, representing R* decay and concurrent G* - PDE* decay, as

$$(6) \qquad \text{PDE}^*(t) = \Phi \cdot \left(\frac{\nu_{\text{RE}}}{k_{\text{R}} - k_{\text{E}}} \right) \left(e^{-k_{\text{E}}(t - t_{\text{RGE}})} - e^{-k_{\text{R}}(t - t_{\text{RGE}})} \right), \quad t > t_{\text{RGE}},$$

where Φ is the number of photoisomerisations per rod per flash, ν_{RE} is the effective rate with which a single R^* triggers activation of PDE^*, and t_{RGE} is the sum of delay time constants, $t_{\mathrm{R}} + t_{\mathrm{G}} + t_{\mathrm{E}}$ (Nikonov et al. 1998).

We refer to (1)-(6) as the "full" model to distinguish it from the following "homogenized" one.

2.4. Homogenized Limit Problem.
The geometry of the rod outer segment exhibits two thin compartments, available to diffusion: the interdiscal spaces and the outer shell surrounding the stack of discs. The diffusion within the interdiscal spaces appears to be prevalent in the transversal directions and it cannot be neglected in view of the reaction terms acting on the faces of the discs. The longitudinal diffusion along the outer shell cannot be neglected because it regulates the opening and closing of the ionic channels. The numerical values of ε_o, R and H (see §4) indicate that $\varepsilon_o \ll R \sim H$. This suggests that ε_o can be regarded as a homogenization parameter to be let go to zero. In doing so the discs C_j within the rod become thinner. We visualize such a process to be carried out in such a way that as $\varepsilon_o \to 0$ the number of discs increases so as the ratio between the volume occupied by the discs and the volume of the rod remains a fixed fraction of 1. On the other hand, the outer shell width is comparable to the mutual distance of adjacent discs. Thus, as $\varepsilon_o \to 0$ the thickness of the outer shell also vanishes and, roughly speaking, the outer shell tends to a cylindrical surface. A suitable device to preserve information on diffusion in the increasingly thinner outer shell is to "concentrate the capacities". For this, the coefficients in the diffusion equation should be changed to compensate the geometrical alteration of the domain, so that the total mass contained in the outer shell stays fixed in the limit.

Andreucci et al. (2003a, 2003b) have developed the homogenized / concentrated capacity limit of the full model by taking $\varepsilon_o \to 0$, $N \to \infty$ while the volume ratio θ_o remains fixed. The homogenized limit problem consists of three pairs of unknowns defined on three different regions: $\{u, w\}$ defined in Ω_o (cylinder of radius R, height H), called the interior limit; $\{\bar{u}, \bar{w}\}$ defined on $\mathcal{D}_R$ (the surface of activated disc(s) at $z = z_0$), called the special level(s) z_0; $\{\widehat{u}, \widehat{w}\}$ defined on $\mathcal{S}$ (the lateral surface at $r = R$), called the limit on the outer shell. The homogenized limit problem in its weak, dimensionless, form can be expressed as (Andreucci et al. 2003a, 2003b; Khanal, 2003)

$$(1 - \theta_o) \int_0^\tau \int_{\Omega_o} \left\{ \frac{\partial u}{\partial t} \psi_1 + D_u \left(\nabla_{\bar{x}} u \cdot \nabla_{\bar{x}} \psi_1 \right) + \left(C_2\, u - C_{\min} - C_1\, f_1(w) \right) \psi_1 \right\}_{z \neq z_0} d\Omega_o\, dt$$

$$+ \sigma \varepsilon_o \int_0^\tau \int_{\mathcal{S}} \left\{ \frac{\partial \widehat{u}}{\partial t} \psi_1 + D_u \left(\nabla_S \widehat{u} \cdot \nabla_S \psi_1 \right) \right\}_{r=R} dS\, dt$$

$$+ \nu \varepsilon_o \int_0^\tau \int_{\mathcal{D}_R} \left\{ \frac{\partial \bar{u}}{\partial t} \psi_1 + D_u \left(\nabla_{\bar{x}} \bar{u} \cdot \nabla_{\bar{x}} \psi_1 \right) + \left(C_2\, \bar{u} - C_{\min} - C_1\, f_1(\bar{w}) \right) \psi_1 \right.$$

$$\text{(7a)} \qquad \left. + \frac{1}{\nu \varepsilon_o} C_0\, \bar{u}\, P \psi_1 \right\}_{z=z_0,\, r \neq R} d\mathcal{D}_R\, dt = 0\,,$$

$$(1 - \theta_o) \int_0^\tau \int_{\Omega_o} \left\{ \frac{\partial w}{\partial t} \psi_2 + D_w \left(\nabla_{\bar{x}} w \cdot \nabla_{\bar{x}} \psi_2 \right) \right\}_{z \neq z_0} d\Omega_o\, dt$$

$$+ \sigma \varepsilon_o \int_0^\tau \int_{\mathcal{S}} \left\{ \frac{\partial \widehat{w}}{\partial t} \psi_2 + D_w \left(\nabla_S \widehat{w} \cdot \nabla_S \psi_2 \right) + \frac{1}{\sigma \varepsilon_o} \left(g_1(\widehat{w}) - C_{\mathrm{ratio}}\, g_2(\widehat{u}) \right) \psi_2 \right\}_{r=R} dS\, dt$$

$$\text{(7b)} \qquad + \nu \varepsilon_o \int_0^\tau \int_{\mathcal{D}_R} \left\{ \frac{\partial \bar{w}}{\partial t} \psi_2 + D_w \left(\nabla_{\bar{x}} \bar{w} \cdot \nabla_{\bar{x}} \psi_2 \right) \right\}_{z=z_0,\, r \neq R} d\mathcal{D}_R\, dt = 0,$$

where ψ_1, ψ_2 are test functions and $\tau > 0$.

Note that the geometry of the homogenized problem is much simpler, involving only the cylinder Ω_o, activated disc(s) z_o, and the surface of Ω_o.

Well-posedness of the full model has been established in Khanal (2003) using upper and lower solutions and their associated monotone iterations. Andreucci et al. (2003b) have established existence and uniqueness for the homogenized problem.

To assess the effectiveness of the homogenized model we have performed numerical simulations with the full model and the homogenized model, as briefly described below. They are compared in Fig.3. Further details and simulations will appear elsewhere.
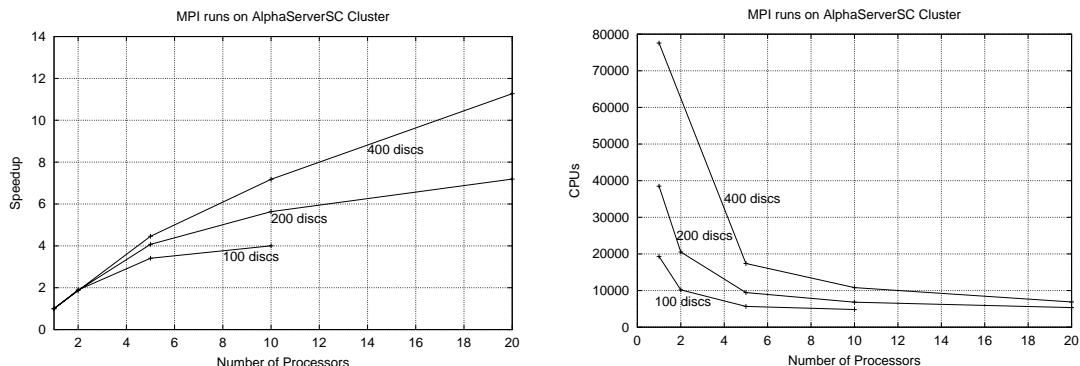
FIGURE 2. Speedup and CPU time (on colt) for 100, 200 and 400 discs.

3. COMPUTATIONAL MODELS

Computational models of the mathematical problems have been developed based on Finite Volume discretization, and implemented in Fortran. We employ explicit-implicit time-stepping, with time-steps sufficiently small to ensure numerical stability of the scheme. Due to the intricate geometry of the cytosol, the problem involves very intensive computations demanding high performance computing.

3.1. Full Model. For the sake of computational efficiency in the full model, we assume axial symmetry to reduce the problem to two space dimensions in (r, z) coordinates. We partition the rod into N small cylinders (disc-units) each of height $\frac{1}{2}\nu\varepsilon_o + \varepsilon_o + \frac{1}{2}\nu\varepsilon_o$, containing one disc placed in the middle. Each disc-unit is discretized into $(I_1 + I_2) \times (2J_1 + J_2)$ control volumes by assigning I_1 nodes in $[0, R]$, I_2 nodes in $[R, R + \sigma\varepsilon_o]$ along the disc radius; J_1 nodes below the disc, J_2 nodes along the height of each disc, and J_1 nodes above the disc.

Parallelization: We parallelized the scheme for distributed memory clusters of processors or heterogeneous networked computers. Since there is no functional parallelism in solving the partial differential equations, the natural data parallelization via domain decomposition has been used. The idea is to decompose the spatial domain into sections and assign a section to each processor. Here a section consists of a group of disc units. The parallel implementation employs the MPI (Message Passing Interface) library, following the master/slaves paradigm generated in SIMD (Single Instruction Multiple Data) mode, where one processor acts as a master and the rest as slaves. The master loads I/O, distributes tasks to the slaves, controls and synchronizes the slaves whereas the slaves all solve the same problem but on their own segment of the mesh, exchange boundary values with their neighbors, and send their output to the master.

Runtime Tests: A serial version of the code tested (for the two dimensional (r, z) axisymmetric case) took 5hr:25min on colt [1] for 1 sec simulation on a coarse grid ($6+4 \times 4+4 = 80$ nodes per disc unit) with 100 discs, which extrapolates to ~ 44 hrs for 800 discs. Note that a typical salamander photoreceptor rod has about 800 discs. Thus parallelization is necessary. To estimate the parallel speed-up we have measured the execution time T_P necessary for performing a fixed computation with N_P processors. Speedup (S) is defined as $S = T_P/N_P$. The parallel performance on colt is depicted graphically in Fig.2. These results are based on the wall clock time of a computation for the same coarse grid (80 nodes per disc unit), and total simulation time 1 sec. Such a run executes 12049753 time-steps. With 10 processors on colt, the 100 disc simulation took 1hr:20min, giving a speedup of 4. As seen in Fig.2 the speedup improves as the size of the problem increases, e.g., 5.63 for 200 discs and 7.18 for 400 discs. This is due to parallel overhead, higher numerical complexity, synchronizations, and non-parallelizable part of the problem.

A typical 1 sec simulation of the full model (axisymmetric case) presented in §5 for a rod with 800 discs, with a fairly fine grid ($64+4 \times 2+2 = 272$ nodes per disc unit) using 21 processors, takes about 8 hours on cheetah [2].

---

[1]colt.ccs.ornl.gov, Compaq AlphaServer SC; compiled with: f90 -fast -O5 -tune ev67 -lfmpi -lmpi -lelan

[2]cheetah.ccs.ornl.gov, IBM pSeries System; compiled with: mpxlf -O4 -qnoipa, run from GPFS area

3.2. **Homogenized Limit Problem.** The computational domain of the homogenized problem (disc-free rod with radius R and height H, with special z-level(s) ($z = z_o$) for activated disc(s)) is discretized into M control volumes V_p, $p = 1, \ldots, M$. We choose the test functions ψ_i, $i = 1, 2$ in (7), as the characteristic function of the closure of a control volume V_p and integrate over each control volume V_p and time interval $[t, t + \Delta t]$. The three pairs of unknowns $\{u, w\}$, $\{\bar{u}, \bar{w}\}$, and $\{\widehat{u}, \widehat{w}\}$ are represented by a single pair $\{U_p^n, W_p^n\}$ for each time level n in each control volume V_p, as the mean values over the control volume. Parallelization can be done as for the full problem.

Exploiting the simpler geometry of the homogenized model, we are currently testing spatially adaptive grids (fine grid near activated disc(s) and coarse grid elsewhere). Early experiments show good improvement in computational efficiency. Implementation details, runtime tests and grid convergence results with adaptive grids will appear elsewhere.

4. SIMULATION SETUP

We obtained some of the parameters from the literature, some by matching terms in our model and the bulk model of Nikonov et al. (2000), Pugh & Lamb (2000), and some by testing many combinations of parameters attempting to match the peak response, and the time at which it occurs, with experimental data of Rieke (2002) on single photon response in salamander rods. Details and parameter values appear in Khanal (2003). Simulations were performed for a typical *salamander* photoreceptor rod with $N = 800$ discs, $R = 5.5\,\mu$m, $\varepsilon_o = \nu\varepsilon_o = 14$ nm, $\sigma\varepsilon_o = 15$ nm and $H = 22.4\,\mu$m. Typical parameters for the whole cell electrical properties at the dark resting state are taken to be $j_{cG}^{max} = 7000$ pA and $j_{ex}^{sat} = 0.17$ pA respectively. The initial state is the dark steady-state with concentrations $u_0 \equiv u_{dark} = 3\,\mu$M, $w_0 \equiv w_{dark} = 0.65\,\mu$M, where u_{dark}, w_{dark} are obtained by solving the system (1) after setting the fluxes in (2) to zero. For the PDE-activation step, the lumped method described in §2 was employed for a flash inducing $\Phi = 1$ photoisomerisation with rate constants $\nu_{RE} = 675$ s^{-1}, $k_E = 0.67$ s^{-1} and $k_R = 2.56$ s^{-1}.

In the simulations reported here, we employ a fairly fine grid of $64+4 \times 2+2 = 272$ control volumes per disc-unit, resulting in $272 \times 800 = 217600$ control volumes for the 800-disc rod. Finer grids were tested, with no discernible effect (to at least 3 significant digits). For the homogenized model, we used the same mesh with additional 4 nodes in θ direction.

The numerical solution of the mathematical models gives the evolution of the spatial distribution of u and w in the cytosol. The local circulating current $J(z, t)$ at any height z at any time t is obtained from (4) using the boundary values of u and w at that z and t. The current $J(t)$ across the entire plasma membrane at time t is the mean value of $J(z, t)$ over $\partial_o \Omega$. At $t = 0$, $J(z, 0) \equiv J(0) =: J_{dark}$, so both the local and total currents can be normalized by J_{dark}. Results are presented in terms of the *normalized response* $1 - J/J_{dark}$ for either local or total J. To quantify the longitudinal spread, we count the number of discs for which response is more than 0.1% of the dark value.

5. NUMERICAL RESULTS

In response to a single photon stimulus ($\Phi = 1$) at the 400th disc of a salamander rod photoreceptor, we obtained 0.53 pA (0.8%) reduction at 800 ms of the 65.97 pA dark current, which agrees with experimental data of Rieke (2002). Longitudinal spread of the response in *salamander* is $4.8\,\mu$m, which amounts to 21.5% of the rod outer segment length ($22.4\,\mu$m). The maximum reduction in local current is 18% (occurring at time 820 ms at the activated 400th disc). The results obtained from the weak form of the homogenized model are compared with the results of the full model in Fig.3. There is good agreement in both the response and spread.

We have verified that activating any single disc farther away than ~ 25 discs from the ends of the rod outer segment produces identical behavior (except, of course, with $z-$profiles shifted at the activation site).

For higher intensity stimulus, when several discs are activated, we observed that the spacing of activated sites significantly affects the response. Activating adjacent discs produces considerably lower response than activating discs far apart from each other. In the simulations shown in Fig.4, with $\Phi = 52$ photoisomerisations, activating seven adjacent discs (discs # 397 - 403) produces 5.5% peak response, whereas activating seven other discs (disc # 100, 200, 300, 400, 500, 600, 700) increases the peak response to 14.5%. Maximal separation (further apart than the spread) produces maximal
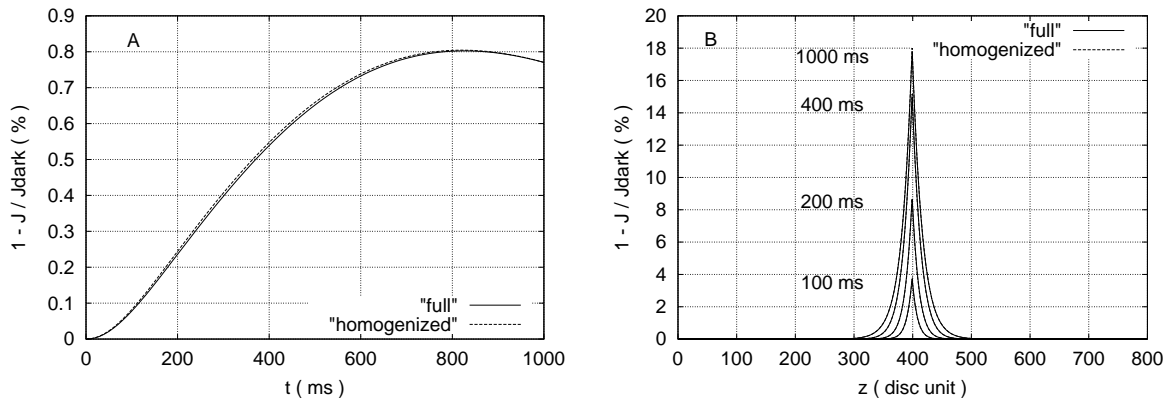
FIGURE 3. Simulations from the "full" and the "homogenized" models of response to a single photon flash delivered at the 400th disc. **(A)** Normalized response $1 - J/J_{\text{dark}}$ versus time. **(B)** Normalized local response $1 - J(z,t)/J_{\text{dark}}$ versus location z at times $t = 100, 200, 400$ and 1000 ms.

response. This phenomenon is difficult to test experimentally, and its physiological significance is currently under investigation.
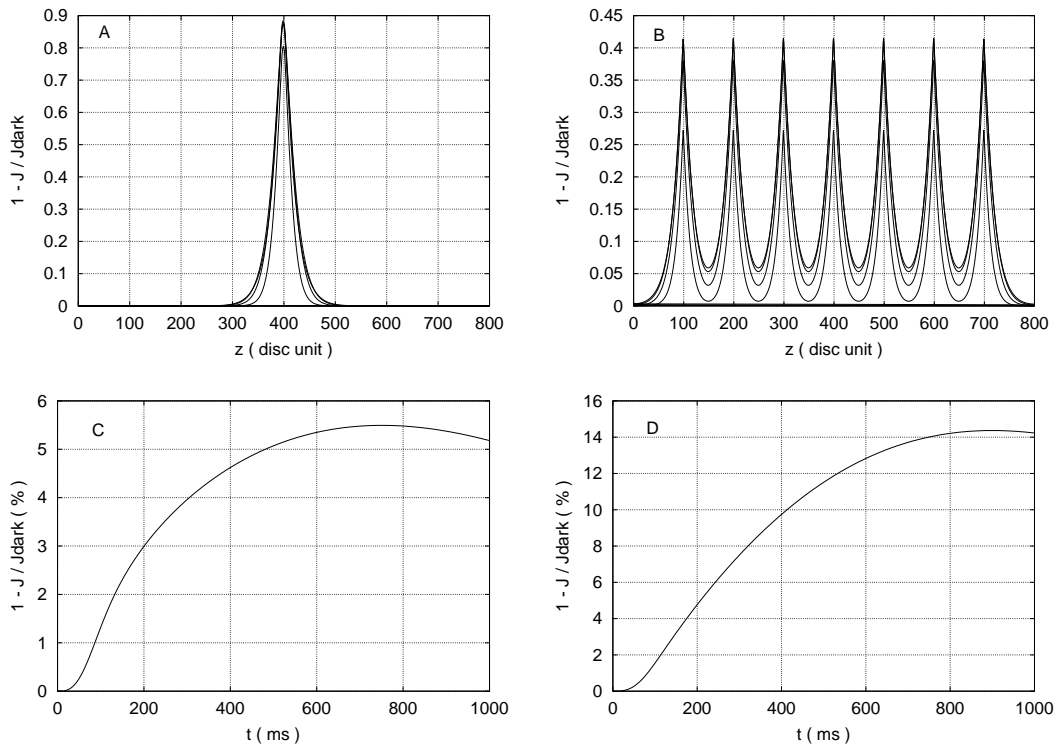

FIGURE 4. Longitudinal spread and histories of normalized responses with different arrangement of activation sites for $\Phi = 52$ photoisomerisations. Seven discs are activated: around the center of the rod (discs # 397 - 403) in **(A)** and **(C)**; 100 discs apart from each other (disc # 100, 200, 300, 400, 500, 600, 700) in **(B)** and **(D)**. **(A)** & **(B)**: Longitudinal spread of (local) relative responses $1 - J(z,t)/J_{\text{dark}}$ at various times. **(C)** & **(D)**: Normalized responses $1 - J/J_{\text{dark}}$ versus time; note the different scales. The suppression of the circulating current varies with the arrangements of the activated discs.

Conclusion: We tested numerically some facts put forth in the biological literature about the response of dark-adapted rod photoreceptors. With appropriate modifications, the model will be useful in studying light and dark adaptation in rods. Numerical simulations, as described here, can be used to test predictions resulting from a specific set of parameters against experimental data. The full model of the complex geometry is implemented in the axisymmetric case. Due to the intricate geometry of the cytosol, even the axisymmetric case of the full model involves very intensive computations. This is achieved via parallelization for distributed memory clusters of processors. The homogenized limit problem is also tested and found to represent the full model. The smoothness of the solution, and almost constant behavior away from the activation site suggest that the homogenized model does not require uniformly fine grids in the axial direction. Thus, we expect adaptive grids to result in considerable computational efficiency, making the homogenized model a highly valuable tool.

ACKNOWLEDGEMENTS

References

[1] D. Andreucci, P. Bisegna, G. Caruso, H.E. Hamm and E. DiBenedetto, Mathematical Model of the Spatio-Temporal Dynamics of Second Messengers in Visual Transduction. *Biophysical J.*, to appear, 2003a.

[2] D. Andreucci, P. Bisegna, and E. DiBenedetto, Homogenization and Concentrated Capacity for a Problem in Visual Transduction. *Annali di Mat. Pura et Appl.* to appear, 2003b.

[3] D.A. Baylor, T.D. Lamb and K.-W. Yau, The Membrane Current of Single Rod Outer Segments. *J. Physiol.*, **288**, pp. 589-611, 1979.

[4] G.L. Fain, H.R. Matthews, M.C. Cornwall and Y. Koutalos, Adaptation in Vertebrate Photoreceptors. *Physiol. Rev.*, vol. 81, No. 1, pp. 117-151, 2001.

[5] M. Gray-Keller, W. Denk, B. Shraim and P.B. Detwiler, Longitudinal Spread of Second Messenger Signals in Isolated Rod Outer Segments of Lizards. *J. Physiol.*, **519**, pp. 679-692, 1999.

[6] R. Hamer, Computational analysis of vertebrate phototransduction: Combined quantitative and qualitative modeling of dark- and light-adapted responses in amphibian rods. *Visual Neuroscience*, **17**, 679-699, 2000.

[7] H. Khanal, Computational models for diffusion of second messengers in visual transduction, *PhD Dissertation*, The university of Tennessee, Knoxville, 2003.

[8] H. Khanal, V. Alexiades, E. DiBenedetto and H. Hamm, Numerical Simulation of Diffusion of Second Messengers cGMP and Ca$^2+$ in Rod Photoreceptor Outer Segment of Vertebrates. In *Unsolved Problems of Noise and Fluctuations in Physics, Biology and High Technology*, editor Sergey Bezrukov, AIP Conference Proceedings 665, American Institute of Physics, pp. 165-172, 2003.

[9] Y. Koutalos, Nakatani, and K.-W Yau, Cyclic GMP Diffusion Coefficients in Rod Photoreceptors Outer Segments. *Biophysical J.*, **68**, pp. 373-382, 1995.

[10] I.B. Leskov, V.A. Klenchin, J.W. Handy, G.G. Whitelock, V.I. Govardovskii, M.D. Bownds, T.D. Lamb, E.N. Pugh, & V.Y. Arshavsky, The Gain of Rod Phototransduction: Reconciliation of Biochemical and Electrophysical Measurements. *Neuron*, **27**, pp. 525-537, 2000.

[11] S. Nikonov, N. Engheta and E.N. Jr. Pugh, Kinetics of Recovery of the Dark-adapted Salamander Rod Photoresponse. *J. Gen. Physiol*, **111**, pp. 7-37, 1998.

[12] S. Nikonov, T.D. Lamb and E.N. Jr. Pugh, The Role of Steady Phosphodiestarase Activity in the Kinetics and Sensitivity of the Light-Adapted Salamander Rod Photoresponse. *J. Gen. Physiol.*, **116**, pp. 795-824, 2001.

[13] E.N. Jr. Pugh and T.D. Lamb, Phototransduction in Vertebrate Rods and Cones: Molecular Mechanisms of Amplification, Recovery and Light adaptation. In *Molecular Mechanism in Visual Transduction*, edited by D.G. Stavenga, W.J. Degrip & E.N. Pugh Jr, Elsevier, Amsterdam, pp. 183-255, 2000.

[14] F. Rieke, Department of Physiology and Biophysics, University of Wasington, Seattle Washington 98195, *personal communication*, Nov. 2002.